THE JOURNAL OF PHYSICAL CHEMISTRY C

Article

Cite This: J. Phys. Chem. C 2018, 122, 540−548

pubs.acs.org/JPCC

# $H_2$ Adsorption on Cu(I)−SSZ-13

Bahar Ipek,*[,†,‡,∥] Rachel A. Pollock,[§] Craig M. Brown,[§,‡] Deniz Uner,[∥] and Raul F. Lobo[†,‡]

[†]Center for Catalytic Science and Technology and [‡]Department of Chemical and Biomolecular Engineering, University of Delaware, Newark, Delaware 19716, United States

[§]National Center for Neutron Research, National Institute of Standards and Technology, Gaithersburg, Maryland 20899, United States

[∥]Chemical Engineering Department, Middle East Technical University, 06800 Ankara, Turkey

Supporting Information

**ABSTRACT:** We report $H_2$ adsorption capacities reaching 0.05 wt % at 303 K and at 1 atm $H_2$ pressure on solid-state CuCl-exchanged [Al]-SSZ-13 and [B]-SSZ-13 zeolites. Differential heat of $H_2$ adsorption is found in the range between 16 and 48 kJ mol $H_2^{-1}$ on Cu(I)-SSZ-13 at 323 K and isosteric heat of adsorption is found between 20 and 55 kJ mol $H_2^{-1}$ on Cu(I)-[B]-SSZ-13 at temperatures between 293 and 323 K. Strong interactions between $H_2$ and the copper cations in Cu(I)-SSZ-13 are evidenced using Rietveld refinements of neutron powder diffraction patterns revealing Cu−deuterium ($D_2$) distances of 2.3(2) and 2.41(1) Å. A temperature-dependent Cu(I) migration—away from the six-membered ring (6MR) and eight-membered ring (8MR)—is related to the high adsorption capacities of the samples at 303 K. At 10 K, access to Cu(I) at 6MR is sterically hindered by framework oxygen atoms (Cu−$O_{framework}$ distance of 2.196(5) Å), rationalizing the low $H_2$ adsorption capacities of Cu(I)-SSZ-13 samples as compared to Na-SSZ-13 at 77 K.


## 1. INTRODUCTION

The identification of environmentally benign sources of energy for transportation and other uses has become a crucial problem given the increasing role of climate change and diminishing oil and gas global reserves. Using $H_2$ as the energy carrier in fuel cell vehicles has the potential to revolutionize the transportation sector provided that efficient storage barriers are resolved. Today, commercial fuel cell electric vehicles use 700 bar compressed $H_2$ storage tanks as onboard storage systems. The ultimate goal in these vehicles is to develop onboard systems with a targeted $H_2$ storage capacity of 5.5 wt % (40 $g_{H2}$ $L_{system}^{-1}$) at near-ambient temperatures and pressures under 100 bar to achieve a driving range greater than 500 km.[1] Using nanoporous adsorbents as $H_2$ storage materials could result in safer and economical $H_2$ storage when compared to compressed vessels (∼700 bar) or cryogenic temperature storage (<20 K) by allowing operation at more moderate conditions. Furthermore, physisorption onto nanoporous materials could supply rapid adsorption kinetics and reversibility, critical properties of good $H_2$ storage materials.

Activated carbons[2,3] and metal−organic frameworks (MOFs)[4−8] having high surface areas (up to 6240 $m^2$ $g^{-1}$ on MOF 210)[5] can achieve $H_2$ storage capacities as high as 8.6 wt % at cryogenic temperatures (and at pressures up to 120 bar).[5] $H_2$ uptakes on MOFs, however, currently do not surpass 1.5 wt % at ambient temperatures (100 bar).[9] While high surface areas and pore volumes—as in MOFs and activated carbons—are essential for $H_2$ adsorption at high $H_2$ pressures (30−120 bar) and at cryogenic temperatures (∼77 K),[1,10] $H_2$ adsorption capacity was directly related to the heat of $H_2$ adsorption at lower pressures[10] and at ambient temperature.[11]

With no dipole and a relatively small quadrupole moment ($2.21 \times 10^{-40}$ C $m^{-2}$),[12] strong hydrogen interaction with the porous adsorbents at ambient conditions depends on the presence of strong polarizing centers. These strong polarizing centers are open metal species in MOFs and extra-framework cations in zeolites and they are the main adsorption sites for hydrogen. On MOFs, one of the highest binding energies reported is 12.3 kJ $mol^{-1}$ g (with an observed $H_2$ bathochromic shift about 135 $cm^{-1}$ in its vibrational frequency) on $Co_2$-*m*dobdc and $Ni_2$-*m*dobdc.[13] Cu(I)-exchanged zeolites, on the other hand, result in $H_2$ adsorption enthalpies between −73 and −39 kJ mol $H_2^{-1}$ and $\nu$(H−H) bathochromic shifts of about 1000 $cm^{-1}$[14] on Cu(I)-ZSM-5,[15] resulting in increased adsorption capacity at ambient temperature.

The strong interaction between $H_2$ and Cu(I) cation on Cu(I)-exchanged zeolites has been explained as the additive effects of the zeolite framework oxygen atoms and electron

Received: October 9, 2017
Revised: December 13, 2017
Published: December 19, 2017





DOI: 10.1021/acs.jpcc.7b09963
J. Phys. Chem. C 2018, 122, 540−548

back-donation from Cu(I) to $H_2$. The framework oxygen atoms, to which Cu(I) cation coordinates, theoretically increase Cu ($3d_\pi$) orbital polarization and reduce Cu(I)−zeolite repulsion which favors Cu(I) ($3d_\pi$) → $H_2$ ($\sigma^*$) back-donation.[16,17] The theoretical binding energy between $H_2$ and Cu(I) adsorption centers in a chabazite framework has been estimated to be between 13 and 56 kJ mol $H_2^{-1}$ by Solans-Monfort et al.[17] These values are lower than the experimental heats of adsorption found on Cu(I)−ZSM-5[15] and are closer to the calculated optimum heat of $H_2$ adsorption of −22 to −25 kJ mol $H_2^{-1}$ for maximum $H_2$ delivery from zeolites.[18] Despite the shown potential of Cu(I)-SSZ-13 for $H_2$ adsorption at ambient conditions, there is no experimental report detailing it.

In this report, samples of Cu(I)-SSZ-13 with different Si/Al ratios have been prepared by solid-state CuCl exchange at various temperatures and investigated for $H_2$ adsorption at both cryogenic and ambient temperatures. The interaction strength of $H_2$ and the prepared zeolites has been investigated using various techniques including microcalorimetry and powder neutron diffraction. As estimated by theory, Cu(I)-exchanged SSZ-13 type zeolites showed differential heat of adsorption values between 48 and 16 kJ $mol^{-1}$ resulting in an improved $H_2$ adsorption capacity (per g of adsorbent) up to 0.05 wt % at a temperature of 303 K and a pressure of 1 atm.

## 2. EXPERIMENTAL SECTION

**2.1. Zeolite Synthesis and Ion Exchange.** SSZ-13 with Si/Al = 6 was prepared hydrothermally as reported by Pham et al.[19] A mixture of 10 g of sodium silicate solution (Sigma-Aldrich, 26.5% $SiO_2$; certain commercial equipment, instruments, and materials are identified in this document. Such identification does not imply recommendation or endorsement by the National Institute of Standards and Technology nor does it imply that the products identified are necessarily the best available for the purpose), 0.32 g of NaOH (Fischer Scientific, > 98%), and 24 g of deionized water was stirred using a magnetic stirrer for 15 min at 298 K. Subsequently, 1 g of Na−Y (Zeolyst CBV100, Si/Al = 2.47) and 1.6 g of *N,N,N*-trimethyl-1-adamantanammonium iodide were added and mixed for 30 min. The white solution was then transferred to a 43 mL Teflon-lined autoclave (Parr) and heated at a temperature of 423 K (under autogenous pressure) for 6 days while the autoclave was tumbled at a rate of 45 rpm. The crystallization product was vacuum filtered and washed with 200 mL of deionized water three times. The recovered solids (2−3 g) were dried at 353 K for 12 h (in air, Fisher Scientific Isotemp Lab Oven) and were calcined in static air at a temperature of 833 K for 8 h using a benchtop muffle furnace (Thermolyne) at a heating rate of 5 K $min^{-1}$. The resulting zeolite is denoted Na/H-SSZ-13/6. (Sample names are given in M-SSZ-13/*xx* format, where M represents the cation type and *xx* represents the Si/Al ratio.)

SSZ-13 with Si/Al = 12 was prepared by stirring 11.81 g of tetraethyl orthosilicate (Sigma, >98%), 23.58 g of *N,N,N*-trimethyl-1-adamantanammonium hydroxide (Sachem Inc., 25 wt %, TMAdaOH), and 2.13 g of deionized water for 2 h at 298 K. After a clear solution was obtained, 0.65 g of aluminum triethoxide (Sigma-Aldrich, 97%, $Al(OEt)_3$) was added slowly and stirred for another 2 h until a final gel composition of 1 $SiO_2$/0.035 $Al_2O_3$/0.5 TMAdaOH/20 $H_2O$ was obtained.[19] The mixture was then transferred to Teflon-lined autoclaves and heated to a temperature of 423 K under static conditions for 7 days. The resulting crystals were recovered using a centrifuge (International Equipment Company, Centra MP4, 4000 rpm for 6 min), washed with deionized water (200 mL for 1 g of zeolite) three times, and dried at 353 K for 3 h (in air, Fisher Scientific Isotemp Lab Oven). The zeolite product was calcined in static air using the same conditions used for Si/Al = 6. The resulting zeolite is denoted $H^+$-SSZ-13/12.

[B]-SSZ-13 was synthesized using the protocol reported by Regli et al.[20] Samples of 8.961 g of *N,N,N*-trimethyl-1-adamantanamine hydroxide (Sachem Inc., 25 wt %, TMAdaOH), 17.5 g of deionized water, and 0.215 g of $H_3BO_3$ (Sigma-Aldrich, >99.5 wt %) were stirred at room temperature for 30 min until a homogeneous mixture was obtained. Then 2.613 g of fumed silica (Cabot Corp., Cab-o-sil M-5) was added to the mixture and stirred for an additional 1 h. The homogeneous mixture was then transferred to a Teflon-lined autoclave (Parr, 43 mL) and heated at 433 K for 6 days with a rotation rate of 75 rpm. The solid product was vacuum filtered, washed with deionized water, and dried at 353 K for 12 h. The as-made product was then calcined at 833 K for 8 h using a heating rate of 3 K $min^{-1}$. The resulting zeolite is $H^+$-[B]-SSZ-13.

$NH_4^+$-ZSM-5 was obtained following the synthesis and ion exchange procedures reported by Yun et al.[21]

**2.2. Ammonium Exchange.** $NH_4^+$-SSZ-13 was obtained by exchanging 1 g of calcined Na/H-SSZ-13/6 in 500 mL of 0.2 M $NH_4NO_3$ (Sigma-Aldrich, > 99%) aqueous solution. The solution was stirred for 3 h at a temperature of 353 K for ion-exchangeand then the zeolite was filtered, washed with 500 mL of deionized water, and dried at a temperature of 353 K in air for 4 h. This exchange procedure was repeated three times.

**2.3. $Na^+$ Exchange.** $NH_4^+$-SSZ-13 was exchanged with $Na^+$ in 500 mL of a 0.1 M $NaNO_3$ (Sigma-Aldrich, >99%) aqueous solution at a temperature of 353 K for 3 h to obtain Na-SSZ-13. The samples were vacuum filtered and washed with deionized water as described in $NH_4^+$ exchange. Na-SSZ-13 samples (Si/Al = 6 and Si/Al = 12) were compared to Cu(I)-SSZ-13 samples as described below.

**2.4. Solid-State CuCl Exchange.** Cu(I) exchange was carried out using solid-state CuCl exchange of $H^+$-SSZ-13 in a quartz flow reactor (Figure S1). A sample of $NH_4^+$-SSZ-13 was dried under vacuum (<67 Pa) at 363 K for 12 h to ensure no water vapor remained inside the zeolite pores. After the dry weight was measured, dehydrated $NH_4^+$-SSZ-13 (300−400 mg) was placed inside a quartz flow reactor having 30 mm diameter and 210 mm length. The temperature of the system was increased to 833 K with a heating rate of 2 K $min^{-1}$. To heat the reactor, a ceramic radiant full cylinder heater from OMEGA (CRFC-26/120-A) and a temperature controller (Cole Parmer, Love controls 16A) were used. The ammonium groups of $NH_4^+$-SSZ-13 were thermally decomposed (eq 1) to give $H^+$-SSZ-13 at 833 K under flow of 50 $cm^3$ $min^{-1}$ He (Keen Gas, 99.999%) flow for 10 h. After the sample was cooled to 373 K, the gas inlet and outlet of the reactor were sealed using close-ended Ultra-Torr vacuum fittings and the reactor was transferred to a dry argon glovebox. A predetermined amount of CuCl (Sigma-Aldrich, 97%), estimated to give Cu(I)/$H^+$ = 1, was dried at a temperature of 353 K under vacuum conditions (<67 Pa) for 12 h and then mixed with the $H^+$-SSZ-13 inside the glovebox using a mortar and pestle for 5 min. The zeolite and CuCl mixture was placed back into the reactor and the reactor was transferred to the synthesis setup and connected to He without being exposed to


DOI: 10.1021/acs.jpcc.7b09963
J. Phys. Chem. C 2018, 122, 540−548

oxygen or water vapor. The quartz reactor was heated initially to 573 K with a heating rate of 2 K $min^{-1}$ and the temperature was maintained at 573 K for 6 h to allow Cu(I) exchange (eq 2). HCl vapor was carried out of the reactor under continuous 50 $cm^3$ $min^{-1}$ He flow.

$$NH_4^+ - \text{SSZ-13} \xrightarrow{\text{He, }\Delta} H^+ - \text{SSZ-13} + NH_3 \quad (1)$$

$$H^+ - \text{SSZ-13} + \text{CuCl} \xrightarrow{\text{He, }\Delta} \text{Cu(I)} - \text{SSZ-13} + \text{HCl} \quad (2)$$

The height of the bed containing the zeolite and CuCl mixture in the reactor did not exceed 5 mm to ensure uniform exchange. After 6 h of reaction, the samples were heated again to a temperature of 823 K (heating rate of 2 K $min^{-1}$) for 10 h to remove any adsorbed CuCl from the sample. Cu(I)-ZSM-5 was also obtained starting from $NH_4^+$-ZSM-5 using the method described above. The Cu-[B]-SSZ-13 sample was treated at 823 K for 9 h. Another Cu(I)-SSZ-13/6 sample was Cu(I)-exchanged at 833 K for 8 h under 50 $cm^3$ $min^{-1}$ He flow, then the temperature was increased to 1023 K at a heating rate of 1 K $min^{-1}$ and kept at 1023 K for 9 h to further reduce the Cl content. The resulting Cu(I)-zeolite samples were transferred to the Ar glovebox and stored there prior to characterization and testing.

**2.5. Analytical Methods.** Samples (exposed to air) were characterized by powder X-ray diffraction using a Phillips X'Pert diffractometer equipped with a Cu K$\alpha$ source ($\lambda$ = 1.5418 Å). The diffractograms were obtained over the 2$\theta$ range of 5 to 50° using a step size of 0.01°. X-ray diffraction (XRD) patterns were also obtained by mixing 0.005 g if standard silicon powder with 0.02 g of zeolite. Measured diffractograms were corrected using Si (111) peak position of 28.465° at $\lambda$ = 1.5418 Å (Si lattice spacing: 5.4307 Å) and analyzed using CelRef Unit-Cell Refinement software,[22] where the unit cell parameters of a rhombohedral unit cell system with a space group $R\bar{3}m$ were refined for the sodium- and copper-exchanged zeolites.

The elemental composition of samples was determined by Inductively Coupled Plasma Optical Emission Spectroscopy (ICP-OES) technique in Galbraith Laboratories, Knoxville, TN. The elemental composition was also obtained using Energy Dispersive X-ray spectra (EDX) with electrons generated using a JEOL JSM 7400F electron microscope operating with an accelerating voltage of 15 kV and a current of 10 $\mu$A.

The textural properties of the Cu(I)-exchanged zeolites were determined using Ar (Keen Gas, 99.999%) adsorption at a temperature of 77 K and using a Micromeritics ASAP 2020 surface area and porosity analyzer since Cu(I)-zeolites bind nitrogen gas ($N_2$) strongly even at room temperature (80 kJ $mol^{-1}$ for Cu(I)-ZSM-5).[23] Na-SSZ-13 samples were characterized with $N_2$ (Keen Gas, 99.999%) adsorption at 77 K after being dehydrated at a temperature of 623 K for 6 h under vacuum (total pressure ~67 Pa). Cu(I)-exchanged zeolites, on the other hand, were vacuum activated at a temperature of 698 K for 6 h. The free space volume was measured using He (Keen Gas, 99.999%) before the analysis. The samples were evacuated (at 0.27 Pa) at room temperature for 2 h in order to fully evacuate He from the pores prior to adsorption measurements. The temperature of the sample during adsorption and free space measurements was set to 77 K using a Dewar filled with liquid $N_2$.

The micropore volume of the prepared samples was calculated using statistical thickness method (t-plot)[24] and Harkins and Jura[25] thickness equation over the thickness range between 3.5 and 5 Å.

**2.6. $H_2$ Adsorption Experiments.** $H_2$ adsorption measurements were carried out using ultra-high-purity-grade $H_2$ (Keen Gas, 99.999%) and a Micromeritics ASAP 2020 instrument. Na-SSZ-13 and Cu(I)-exchanged (powder, ~150 mg) were pretreated at 623 and 698 K, respectively, for 6 h in vacuo (67 Pa, at the degas port of Micromeritics ASAP 2020 instrument) prior to $H_2$ adsorption to eliminate water or other adsorbates. The sample containers were backfilled with Ar at room temperature after the degassing was completed. After the sample containers were transferred to the analysis port, the zeolites were further evacuated at a temperature of 698 K for 15 min to completely desorb Ar. Evacuation at 0.27 Pa continued for 45 additional minutes at room temperature. Free space volume measurement was performed as explained in the pore volume characterization section. During the adsorption experiments and free space measurements, the temperature of the samples was controlled using liquid $N_2$ (77 K) filled Dewar or an ethylene glycol−water mixture bath. The temperature of the ethylene glycol-water mixture was controlled using a temperature controller (LAUDA Alpha RA 12).

$H_2$ adsorption isotherms were obtained for pressures between 0.01 atm (1.3 kPa) and 1 atm (101.3 kPa). The absolute $H_2$ adsorption amounts were reported in mmol $H_2$ per gram of zeolite. The excess $H_2$ adsorption amounts for tested samples were calculated using eq 3

$$q_{ex} = q - \rho_H V_a \quad (3)$$

where $q_{ex}$ is the excess $H_2$ adsorption amount (mmol $H_2$ $g_{zeolite}^{-1}$), $q$ is the absolute adsorption amount (mmol $H_2$ $g_{zeolite}^{-1}$), $\rho_H$ is the bulk density of $H_2$ at adsorption pressure and temperature (0.03913 mmol $cm^{-3}$ at 303 K and 1 atm), and $V_a$ is the pore volume of the adsorbent, which was determined experimentally.

**2.7. Microcalorimetry Measurements.** Differential heat of adsorption measurements were conducted on a Setaram C-80 Tian−Calvet calorimeter coupled to the multiport high-vacuum Pyrex glass manifold backed by a turbo molecular pump (Pfeiffer, TMH 065) and a diaphragm pump (Pfeiffer, MVP 015).[26] The pressure was measured by a pressure gauge (mks Baratron Capacitance Manometer) in the range of 1.3−133.3 kPa. Approximately 200 mg of air-exposed Cu(I)-SSZ-13 was loaded into the Pyrex sample cell and inserted into the sample port of the microcalorimeter. The sample was treated in situ at 523 K (using a heating rate of 5 K $min^{-1}$) for 13 h and cooled to 323 K under vacuum before the free space measurement. The free space inside the sample cell and the sample was calculated by dosing 18.3 kPa of He (Oksan, > 99.9%) inside a known volume of 152 mL and then expanding it to the sample cell at 323 K. After the sample was degassed at 323 K for 1 h, differential heats of $H_2$ adsorption were measured by introducing 1.7−22.7 kPa of $H_2$ (Oksan, >99.9%) into the sorption chamber at 323 K. Since the increments of gas were added to the sample cell by opening the valve between the dosing cell and the sample cell for each loading, the gas inside the dosing cell expands while the gas inside the sample cell is compressed by the incoming gas. Therefore, the differential heat of adsorption value must be corrected by subtracting the released heat related to this expansion and compression. To estimate the heat due to the expansion and


DOI: 10.1021/acs.jpcc.7b09963
J. Phys. Chem. C 2018, 122, 540−548

compression, an empirical relationship between $Q_{ex}$ (the extra heat term in J) and $\Delta P$ (the pressure difference between the dosing cell and the sample cell) was obtained by dosing $H_2$ into the empty sample cell (see the Supporting Information).

**2.8. Powder Neutron Diffraction (pND) Experiments.** pND experiments were conducted on instrument BT1, the high-resolution diffractometer, at the National Institute of Standards and Technology Center for Neutron Research, Gaithersburg, MD. The wavelength was selected using a Ge(311) monochromator with an in-pile 60′ collimator ($\lambda$ = 2.0787(2) Å). Patterns were collected using 32 He detectors over the $2\theta$ range of 1.3−166.3° with 0.05° step size. Cu(I) SSZ-13 (Si/Al = 6, 0.891 g) was pretreated at 698 K for 6 h and placed into a cylindrical Vanadium can in a dry He box. The vanadium can was sealed with an indium O-ring. Residual He inside the vanadium can was removed using a turbo molecular pump prior to the diffraction experiment. The temperature of the sample was set to 10 and 300 K using a closed cycle He refrigerator.

$D_2$ adsorption onto pretreated samples was performed by calculating the precise amount of $D_2$ need to achieve $D_2$/Cu = 0.5. $D_2$ was loaded at 300 K and then cooled to 10 K for the diffraction experiment.

Rietveld refinement of the collected pND data were performed using the GSAS[27] package along with EXPGUI (graphical user interface).[28] In the Rietveld refinement of the pND data, a hexagonal unit cell with the space group $R\bar{3}m$ was used. Cu(II)-SSZ-13 (Si/Al = 12) pND data was used as starting atomic coordinates for chabazite (CHA) framework.[29] After setting the experimental background manually, it was fitted using Shifted Chebyschev equations using 12 parameters. Peak profile terms (using pseudo-Voigt function with Finger−Cox−Jephcoat asymmetry) and unit cell parameters were fitted using Le Bail method. Atomic positions, occupancies, and thermal displacement parameters (U) were then fitted using Rietveld refinement and using soft constraints on tetrahedral bond lengths (T−O). The tetrahedral bond length (T−O) was set to 1.61 ± 0.03 with the restraint weight of 50. The occupancies of each framework and extra-framework atom were refined without using constraints for the diffraction data obtained with $D_2$ loading. Cu occupancies for bare Cu-SSZ-13 were then fixed to the refined values obtained from diffraction data with $D_2$ adsorption.

## 3. RESULTS AND DISCUSSION

**3.1. Material Characterization.** Characterization of Na-SSZ-13 and Cu(I)-SSZ-13 samples by powder X-ray Diffraction showed that Cu(I)-SSZ-13 and Na-SSZ-13 zeolites were pure chabazite samples with high crystallinity (Figure 1). The solid-state exchange of CuCl and further heating up to a temperature of 1023 K did not result in degradation of the samples' XRD patterns. Refined rhombohedral unit cell parameters ($a$, $\alpha$) for Na and Cu(I)-exchanged zeolites are given in Table S1. Na- and Cu(I)-SSZ-13 with an Si/Al ratio of 6 have higher unit cell volumes (805 and 799 Å$^3$, respectively) than Na- and Cu(I)-SSZ-13 with an Si/Al ratio of 12 (785 and 786 Å$^3$ respectively) due to higher concentration of Al having longer Al−O bonds in SSZ-13 (Si/Al = 6) ($d_{Al-O}$: 1.73 Å and $d_{Si-O}$: 1.61 Å).[30] Cu-[B]-SSZ-13, on the other hand, has a smaller unit cell volume (767 Å$^3$) due to shorter B−O bonds ($d_{B-O}$: 1.51 Å)[31] than Si−O bonds.

Commonly used Cu-exchange methods on zeolites are Cu(II) exchange in aqueous solutions and the solid-state[32,33]

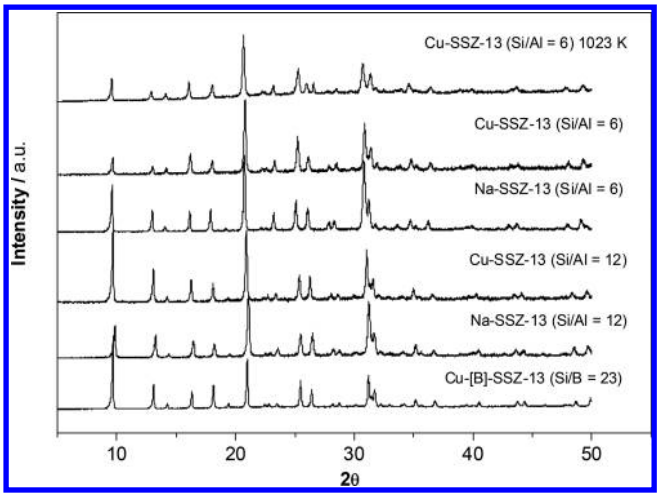


**Figure 1.** Powder XRD pattern of Na-SSZ-13 (Si/Al = 6 and 12), Cu-SSZ-13 (Si/Al = 6 and 12), and Cu−[B]-SSZ-13 (Si/B = 23), Cu K$\alpha$, $\lambda$ = 1.5418 Å.

or vapor-phase[14,34−37] exchange of Cu(I) salts. Cu(II) exchange in aqueous solutions results in Cu(II)/Al ratios always smaller than 1 due to the Cu(II) exchange near two Al sites. It is possible to achieve Cu(I) exchange extents of up to Cu(I)/Al = 1[32] using the solid-state or vapor-phase exchange of CuCl. Here, solid-state Cu(I) exchange of SSZ-13 resulted in 97% and 98% Cu(I) exchange for Si/Al = 6 and Si/Al = 12 samples (Table S2), equivalent to 13.2 and 8.6 wt % Cu (2.07 and 1.33 mmol Cu g$^{-1}$) respectively.

The reaction between the Brønsted acid sites of ZSM-5 and CuCl occurs at a temperature of 573 K based on the observation of HCl vapor at that temperature.[38] However, the solid-state or vapor-phase exchange of CuCl results in residual Cl inside the zeolite pores.[33,36,39] Solid-state CuCl-exchanged ZSM-5 (Si/Al = 11) contains 0.48 Cl/Al even after 40 h heat treatment in He at the temperature of 823 K.[40] Chlorine was also observed in the final product for all Cu(I)-exchanged samples prepared here. One way to decrease the concentration of Cl residuals is to flow an inert gas at high temperature after the CuCl exchange.[33] We found that 10 h treatment at a temperature of 823 K was not sufficient to eliminate all the CuCl occluded in the crystals. Increasing the treatment temperature to 1023 K for CuCl exchange of SSZ-13 (Si/Al = 6), on the other hand, resulted in a lower chlorine content (Cl/Al = 0.06), together with lower Cu(I) present in the sample (Table S2).

A lower concentration of Na in SSZ-13/12 resulted in a higher available micropore volume (0.265 cm$^3$ g$^{-1}$) for adsorption compared to Na-SSZ-13/6 (0.233 cm$^3$ g$^{-1}$) (see Table 1 and Table S2). For Cu(I)-exchanged samples, chlorine together with high Cu(I) concentration reduced the micropore volumes (0.183 cm$^3$ g$^{-1}$) with respect to those of Na-exchanged zeolites. Higher micropore volumes were observed with lower Cu content as in Cu(I)-[B]-SSZ-13 sample (0.248 cm$^3$ g$^{-1}$).

**3.2. $H_2$ Adsorption Isotherms.** At 303 and 77 K, Cu(I)-SSZ-13/6 and Na-SSZ-13/6 showed higher $H_2$ adsorption capacity on a per gram basis than Cu(I)-SSZ-13/12 and Na-SSZ-13/12 due to the higher concentrations of Na and Cu(I) cations (see Figure 2). When the $H_2$ adsorption capacity per mol of Cu cation was calculated, Cu(I)-SSZ-13/6 and Cu(I)-SSZ-13/12 had comparable adsorption capacities at similar


DOI: 10.1021/acs.jpcc.7b09963
J. Phys. Chem. C 2018, 122, 540−548

**Table 1. Total and Excess $H_2$ Adsorption Amounts per Gram of Adsorbent and per $cm^3$ of Pore Volume at an Equilibrium Pressure of 1 atm and Temperature of 303 K**

| adsorbent | total adsorption (mmol $H_2$ $g^{-1}$) | excess adsorption (mmol $H_2$ $g^{-1}$) | micropore volume ($cm^3$ $g^{-1}$) | excess adsorption (mol $H_2$ $mol^{-1}$ Cu) | excess adsorption (mmol $H_2$ $cm^{-3}$) | ref |
|---|---|---|---|---|---|---|
| Cu(I)−[B]-SSZ-13 | 0.250 | **0.240** | 0.248 | 0.522 | 0.968 | *a* |
| Cu(I)-SSZ-13/6-1023 K | 0.232 | **0.223** | 0.239 | 0.158 | 0.933 | *a* |
| Cu(I)-SSZ-13/6 | 0.208 | **0.201** | 0.182 | 0.097 | 1.104 | *a* |
| Na(I)-SSZ-13/6 | 0.077 | 0.068 | 0.233 | 0.027 | 0.292 | *a* |
| Cu(I)-SSZ-13/12 | 0.120 | 0.113 | 0.183 | 0.085 | 0.617 | *a* |
| Na(I)-SSZ-13/12 | 0.0220 | 0.012 | 0.265 | 0.010 | 0.045 | *a* |
| Cu(I)−ZSM-5/12 | 0.185 | 0.181 | 0.113 | 0.190 | 1.602 | *a* |
| Cu(I)-ZSM-5/22[b] | 0.201 | | | | | 14 |
| MOF-177[c] | | 0.160 | 1.720 | | 0.093 | 42 |
| MOF-5[d] | 0.096 | | | | | 7 |
| Fe-BTT[e] | 0.115 | 0.020 | 0.715 | | 0.028 | 43 |

[a]Adsorption at 1 atm and 303 K, this work. [b]Adsorption at 1 atm and 293 K. [c]Adsorption at 4.3 bar and 298 K. [d]Adsorption at 5.2 bar and 298 K. [e]Adsorption at 2.09 bar and 298 K.

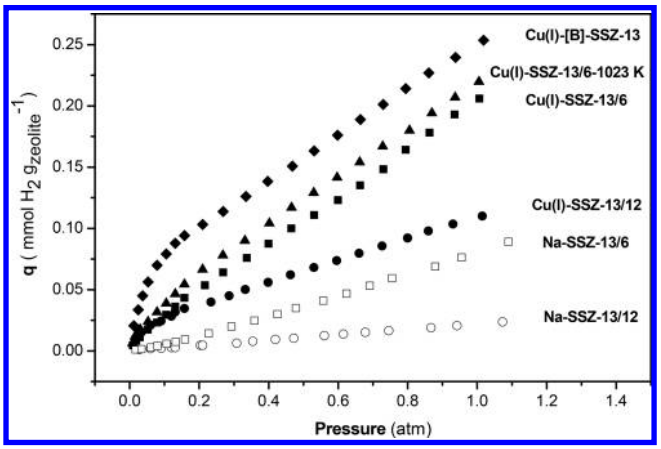


**Figure 2.** $H_2$ adsorption isotherms for Na−- and Cu(I)−-SSZ-13 samples at 303 K. Sample names are given in M-SSZ-13/*xx* format, where M represents the cation type and *xx* represents the Si/Al ratio.

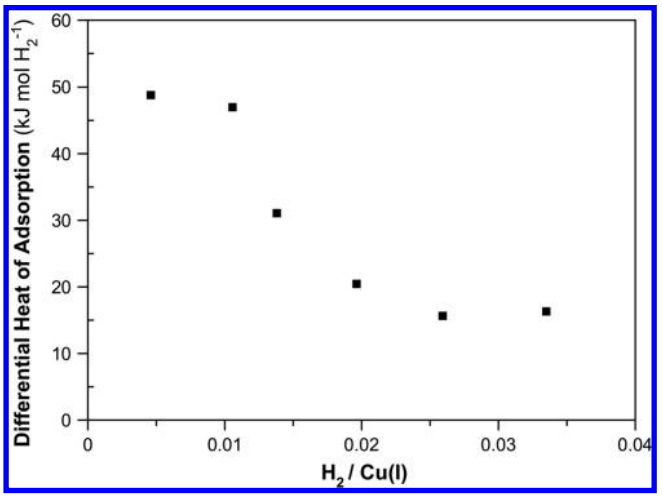


**Figure 3.** Differential heat of $H_2$ adsorption on Cu(I)-SSZ-13/6 obtained using a Tian−Calvet-type microcalorimeter at 323 K.

conditions (0.097 versus 0.085 respectively, Table 1). At 303 K, Cu(I)-[B]-SSZ-13 showed remarkable $H_2$ adsorption capacity both per gram basis ($q$, mmol $H_2$ $g^{-1}$) and per mol of Cu (mol $H_2$ $mol^{-1}$ Cu), reaching 0.05 wt % $H_2$ adsorption capacity at 1 atm $H_2$ pressure.

$H_2$ adsorption capacity of metal organic frameworks and other potential $H_2$ adsorbents is not often reported at room temperature and at atmospheric pressure. Instead, adsorption capacities at higher pressures compensate for the low adsorption enthalpy values (−4 to −12 kJ $mol^{-1}$) observed on metal organic frameworks.[41] Therefore, $H_2$ adsorption capacities of zeolites obtained at room temperature and 1 atm $H_2$ pressure here are compared to those for the metal organic frameworks at higher pressures (Table 1).

Cu(I)-SSZ-13/6, Cu(I)-SSZ-13/6-1023 K, and Cu(I)-[B]-SSZ-13 samples showed total and excess $H_2$ adsorption capacities (per gram basis) that are higher than Cu(I)-ZSM-5 at 1 atm and still higher than those of MOF-5, MOF-177, and Fe-BTT at pressures higher than 2 bar (>0.201 mmol $H_2$ $g^{-1}$ on Cu(I)-SSZ-13/6 at 1 atm versus 0.096, 0.160, and 0.115 mmol $H_2$ $g^{-1}$ at $P$ > 2 bar, Table 1).

The differential heat of $H_2$ adsorption was found between 48 and 16 kJ mol $H_2^{-1}$ for Cu(I)-SSZ-13/6 (Figure 3) at 323 K between pressures of 1.2 kPa (~0.01 atm) and 20.3 kPa (0.2 atm). The observed differential heats are remarkably close to the theoretically calculated $H_2$ binding energies at the Cu(I) sites on the 8MR (56 kJ $mol^{-1}$) and on the 6MR, respectively (13 kJ $mol^{-1}$),[17] even though observed values could still represent the statistical averages of adsorption heats at different adsorption sites. Note that the heat of adsorption stabilizes around 16 kJ mol $H_2^{-1}$ after 9 kPa (corresponding $H_2$/Cu ratio of 0.02) indicating a dominant binding energy of 16 kJ $mol^{-1}$, which is close to the optimal $H_2$ adsorption enthalpies for zeolites (−22 to −25 kJ $mol^{-1}$) determined for maximum $H_2$ delivery by adsorption at a loading pressure of 30 bar and desorption at 1.5 bar at ambient temperature.[18] Observed differential heats of $H_2$ adsorption on Cu(I)-SSZ-13 are greater than the low adsorption enthalpy (−4 to −12 kJ $mol^{-1}$) found for metal organic frameworks. This is consistent with the larger adsorption capacity of Cu(I)-SSZ-13 at ambient conditions.

The isosteric heat of adsorption was also investigated for Cu(I)-[B]-SSZ-13 at constant $H_2$ loadings between 0.04 and 0.37 $H_2$/Cu(I) (at temperatures between 303 and 323 K) and found to be between 20 and 55 kJ $mol^{-1}$ (Figure S5). When the two samples are compared on a $H_2$/Cu basis, the $H_2$ binding energy on Cu(I)-[B]-SSZ-13 is higher than Cu(I)-SSZ-13, showing an isosteric heat of adsorption of about 50 kJ $mol^{-1}$ for $H_2$/Cu ratio from 0.04 to 0.15, which levels off to ~20 kJ $mol^{-1}$ at $H_2$/Cu loading of 0.39. This higher binding



DOI: 10.1021/acs.jpcc.7b09963
J. Phys. Chem. C 2018, 122, 540−548

energy is consistent with the higher $H_2$ adsorption capacity of Cu(I)-[B]-SSZ-13 when compared to Cu(I)-SSZ-13 at 303 K (see Figure 2).

At the temperature of 77 K, $H_2$ adsorption capacities of Cu(I)-exchanged zeolites were compared to Na-SSZ-13/6 and Na-SSZ-13/12 (Figure S6) and to MOF-5, MOF-177, IRMOF-8, and IRMOF-11 (Table S5). Cu(I)-[B]-SSZ-13 and Cu(I)-SSZ-13/6−1023 K resulted in capacity values at 1 atm higher than MOF-5, MOF-177, and comparable to IRMOF-8 and IRMOF-11 (1.34 wt % $H_2$ on Cu(I)-SSZ-13/6−1023 K versus 1.60 wt % $H_2$ on IRMOF-11) despite the lower pore volumes of zeolites. At this temperature, more notably in the lower pressure region, Na-SSZ-13/6 and Na-SSZ-13/12 adsorbed more $H_2$ molecules than Cu(I)-exchanged samples with the exception of Cu(I)-SSZ-13/6−1023 K and Cu(I)-[B]-SSZ-13 at higher pressures (Figure S6). The higher adsorption capacity of Cu(I)-exchanged samples at 303 K than at 77 K are explained in terms of temperature-dependent cation migration in the next section.

**3.3. Powder Neutron Diffraction (pND).** Cation locations on the CHA framework have been reported (i) at the center of the d6MR (site I), (ii) at the 6-ring of the d6MR (site II), (iii) at the window of the 4MR (site III), and at the window of the 8MR (site III′).[44]

We investigated Cu(I) cation location and the unit cell parameters of Cu(I)-SSZ-13/6 using powder neutron diffraction at 10 K (see Table S7) and at 300 K (Table S8) in vacuo and after $D_2$ adsorption (Table S9). Two Cu locations were identified by Rietveld refinement for Cu(I)-SSZ-13/6 at these conditions. At 10 K, copper was observed in site II (Cu1), centered between three O1 atoms with a mean distance of 2.196(5) Å, and another copper was observed in site III′ (Cu2, Figure 4) with Cu1/Cu2 ratio of 0.91. At this

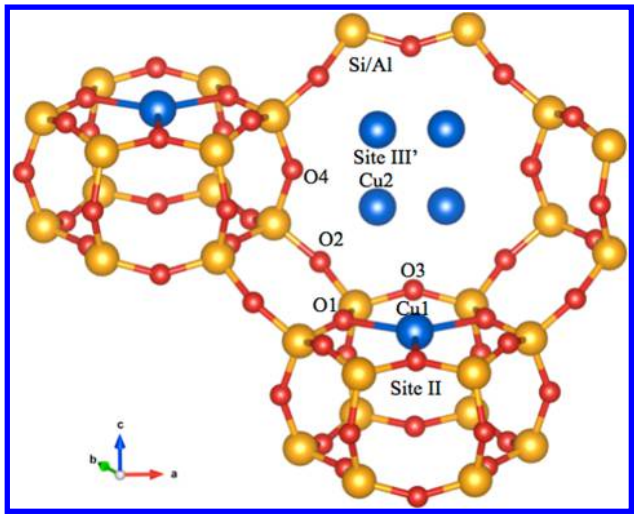


**Figure 4.** Illustration of Cu(I)-SSZ-13 (Si/Al = 6) with two copper positions: Cu1 at site II and Cu2 at site III′.

temperature, Cu1 was displaced 0.04 Å away from the plane of O1 atoms in the ***c*** axis of the hexagonal unit cell. The second Cu(I) site was at the window of 8MR (site III′) (Cu2) with a Cu2−O2 distance of 2.21(6) Å (Table 2), close to 2.06 Å calculated for the second most preferable (stable) location of copper cation using B3LYP periodic methods.[17]

At 300 K, a 11.1 $Å^3$ of decrease in the unit cell volume (i.e., a negative thermal expansion) was observed with cell parameters

**Table 2. Bond Distances and Unit Cell Parameters Obtained via Rietveld Refinement of pND Data of Bare Cu(I)-SSZ-13 (Si/Al = 6, $Cu_5Al_{5.14}Si_{30.86}O_{72}$) at 10 and 300 K and pND Data Obtained at 10 K with $D_2$ Loading at 300 K, $R\bar{3}m$[a]**

| | bare, 10 K | $D_2$ loading, 10 K | bare, 300 K |
|---|---|---|---|
| Cu1−O1 | 2.196(5) | 2.224(6) | 2.195(6) |
| Cu2−O2 | 2.21(6) | 2.22(2) | 2.28(3) |
| Cu2−O4 | | | 2.3(1) |
| Cu1−D1 | | 2.3(1) | |
| Cu2−D2 | | 2.41(1) | |
| Cu3−D3 | | 2.3(2) | |
| | | | |
| $a$ (Å) | 13.6197(5) | 13.6235(5) | 13.6055(5) |
| $c$ (Å) | 15.0546(8) | 15.0332(9) | 15.0169(9) |
| $V$ ($Å^3$) | 2418.4(2) | 2416.4(2) | 2407.3(2) |
| $\chi^2$ | 1.170 | 1.025 | 0.9957 |
| $R_p$ (%) | 4.73 | 4.25 | 4.58 |
| $wR_p$ (%) | 5.75 | 5.27 | 5.56 |

[a]Values in parentheses indicate one standard deviation in the prior digit.

of $a$ = 13.6055(5) Å and $c$ = 15.0169(9) Å (Table 2). At this temperature, the Cu(I) cation at site II and four oxygen atoms were refined using anisotropic Debye−Waller factors. The Cu(I)−O1 distance was 2.195(6) Å with a 0.19 Å displacement from the O(1) plane (larger than the 0.04 Å found at 10 K). Cu2−O2 and Cu2−O4 distances refined to 2.28(3) and 2.3(1) Å (Table 2), longer at 30 K than at 10 K. These more exposed locations of Cu(I) cations (that migrated toward the chabazite cage) at site III′ and the anisotropic movement of Cu1 at site II with increased thermal energy are likely the origin of the higher adsorption capacity of Cu(I)-SSZ-13 at 303 K than at 77 K.

$H_2$−Cu(I) interactions were investigated by loading $D_2$ on Cu(I)-SSZ-13 at 300 K. Two different Cu(I) locations near site II were observed from the neutron diffraction data obtained at 10 K. One site (Cu1) was at the plane of the O1 atoms of the 6MR, and another Cu(I) cation (Cu3) was observed 1.1 Å away from the 6MR window (Figure 5). This unexpected migration of Cu3 away from site II is probably related to the strong interaction of Cu(I) with $D_2$, resulting in Cu3−D3 bonds with a refined distance of 2.3(2) Å. Another interaction was observed between D2 and Cu2 (at the 8MR window, site III′) with Cu2−D2 distance of 2.41(1) Å (Table 2). The refined Cu−D distances in our samples are comparable to the 2.23(5) Å found for $Co_2$(*m*-dobdc) where an isosteric heat of adsorption of 11.5 kJ $mol^{-1}$ was calculated.[13] The large standard deviations in the refined Cu−D distances prevents the comparison of the $D_2$ and Cu(I) interaction strength at site II and site III′.

Accessibility of the extra-framework cation to $H_2$ is as important as Cu(I) distribution for the determination of $H_2$ adsorption capacity. Half of the copper cations in Cu(I)-SSZ-13/6 were found at site II. At 10 K, Cu(I) at site II was 0.04 Å away from the O1 plane with the Cu−O distance of 2.196(5) Å. Using a 1.35 Å Shannon radii for the oxygen framework atom and 0.6 Å radii for the Cu(I) cation, it appears that the majority of Cu(I) cations are shielded by $O_{fw}$ atoms at low temperatures. Sodium cations, on the other hand, having a Shannon radii of 1.02 Å, were located 0.83 Å away from O(1) atomic plane.[45] At this position, $H_2$ can easily adsorb on the



DOI: 10.1021/acs.jpcc.7b09963
J. Phys. Chem. C 2018, 122, 540−548

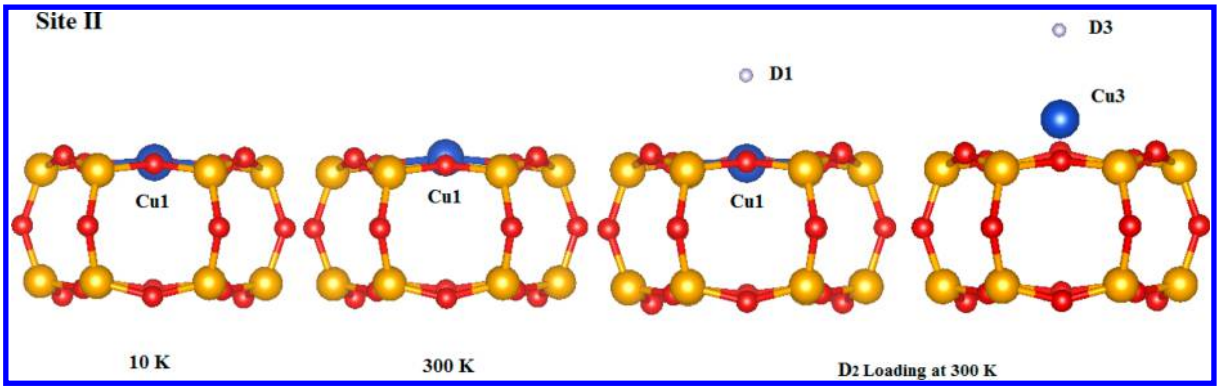


**Figure 5.** Illustration of Cu(I) at site II determined from pND measurements of Cu(I)-SSZ-13/6 at 10, 300, and at 10 K following $D_2$ loading at 300 K.

Na cation at site II unlike Cu cation. This difference explains the higher $H_2$ adsorption capacities observed for Na-SSZ-13 than for Cu(I)-SSZ-13 at 77 K (Figure S6).

The anisotropic atomic displacement factors of Cu(I) cation at site II (along [001]) together with the 0.19 Å displacement from the O(1) plane at 300 K indicate a detachment of the Cu(I) cations from the O atom shielding, which resulted in stronger interaction of Cu(I) and $D_2$ and a guest-induced Cu(I) migration (1.1(2) Å, Figure 5) at site II. Guest-induced cation migration is not uncommon for Cu(I)-containing zeolites (such as Cu(I)−Y). For example, Palomino et al. reported displacement of Cu(I) cations up to 0.975 Å in the presence of CO at 80 K.[37] Shang et al. suggested that the degree of guest-induced migration is related to the electronic quadrupole moments and polarizability of the guest molecules that could increase the cation-guest molecule interaction.[46] In our case, formation of Cu−$H_2$ complexes renders $H_2$ a potential "strong" guest molecule especially at near room temperature, which explains high $H_2$ adsorption capacities of Cu(I)-SSZ-13 zeolites at 303 K (Figure 2). This realization can be used as a guiding principle for the design of improved $H_2$ adsorbents on Cu(I) containing materials.

## 4. CONCLUSIONS

Improved $H_2$ storage to fulfill the targets set for the fuel-cell vehicles requires adsorbent properties like high surface area and a large heat of adsorption to increase the $H_2$ adsorption capacity at practical conditions. We have showed that an optimal heat of adsorption is viable on Cu(I)-exchanged SSZ-13 that improves the $H_2$ adsorption capacity up to 0.05 wt % at a temperature of 303 K and a pressure of 1 atm. The differential heat of adsorption and the isosteric heat of $H_2$ adsorption values between 16 kJ mol $H_2^{-1}$ and 55 kJ mol $H_2^{-1}$ enabled $H_2$/Cu ratios on Cu(I)-SSZ-13 and Cu(I)-[B]-SSZ-13 reaching 0.5 (0.05 wt % capacity) at these conditions.

Powder neutron diffraction studies reveal two different Cu(I) sites; one at the 6-ring window of the d6MR and one at the window of the 8MR. Strong $H_2$ interactions with Cu(I) cations are confirmed by identified $D_2$ adsorption sites at 300 K, which resulted in Cu−D distances as short as 2.3(2) Å.

The effect of temperature on the molecular structure of Cu(I)-SSZ-13 was monitored using pND, and we found that at lower temperatures (10 K) Cu(I) cations at the window of the 6-membered ring were shielded by framework oxygen atoms with Cu−$O_{framework}$ distances of 2.196(5) Å, resulting in lower $H_2$ adsorption capacities than Na-SSZ-13 at 77 K. At a more practical operating temperature of 303 K, these Cu(I) cations were observed to migrate toward the chabazite cage and become more accessible by $H_2$ molecules. Therefore, if $H_2$ storage systems were operated at lower temperatures aiming for higher $H_2$ adsorption capacity, investigation of zeolites excluding 6-membered rings is required. However, at 303 K, for Cu(I) the shielding effect of the neighboring oxygen atoms becomes negligible by the temperature dependent Cu migration, making Cu-SSZ-13 a potential $H_2$ storage material at around room temperature with optimal $H_2$ interaction strength.

## ■ ASSOCIATED CONTENT

### Supporting Information

The Supporting Information is available free of charge on the ACS Publications website at DOI: 10.1021/acs.jpcc.7b09963.

CuCl-exchange set-up, further sample characterization, heat of adsorption calculations, (4) $H_2$ adsorption data at 77 K, (5) powder neutron diffraction results (PDF)

Rietveld refinement results for Cu(I)-SSZ-13 (Si/Al = 6) at 10 K (CIF)

Rietveld refinement results for Cu(I)-SSZ-13 (Si/Al = 6) at 300 K (CIF)

Rietveld refinement results for Cu(I)-SSZ-13 (Si/Al = 6) at 10 K following $D_2$ loading at 300 K (CIF)

## ■ AUTHOR INFORMATION

### Corresponding Author

*E-mail bipek@metu.edu.tr.

### ORCID

Bahar Ipek: 0000-0002-0584-2296

Raul F. Lobo: 0000-0003-4027-3129

### Author Contributions

The manuscript was written through contributions of all authors. All authors have given approval to the final version of the manuscript.

### Notes

The authors declare no competing financial interest.

## ■ ACKNOWLEDGMENTS

This manuscript was prepared under cooperative agreement 70NANB12H239 from the National Institute of Standards and Technology (NIST), U.S. Department of Commerce. We acknowledge the support of the National Institute of Standards and Technology, U.S. Department of Commerce, in providing



DOI: 10.1021/acs.jpcc.7b09963
J. Phys. Chem. C 2018, 122, 540−548

the neutron research facilities used in this work. This work utilized facilities supported in part by the National Science Foundation under Agreement No. DMR-0944772. The statements, findings, conclusions and recommendations are those of the authors and do not necessarily reflect the view of NIST or the U.S. Department of Commerce.

## REFERENCES

(1) Broom, D. P.; Webb, C. J.; Hurst, K. E.; Parilla, P. A.; Gennett, T.; Brown, C. M.; Zacharia, R.; Tylianakis, E.; Klontzas, E.; Froudakis, G. E.; et al. Outlook and Challenges for Hydrogen Storage in Nanoporous Materials. *Appl. Phys. A: Mater. Sci. Process.* **2016**, *122*, 151.

(2) Texier-Mandoki, N.; Dentzer, J.; Piquero, T.; Saadallah, S.; David, P.; Vix-Guterl, C. Hydrogen Storage in Activated Carbon Materials: Role of the Nanoporous Texture. *Carbon* **2004**, *42*, 2744−2747.

(3) Panella, B.; Hirscher, M.; Roth, S. Hydrogen Adsorption in Different Carbon Nanostructures. *Carbon* **2005**, *43*, 2209−2214.

(4) Hirscher, M. Hydrogen Storage by Cryoadsorption in Ultrahigh-Porosity Metal-Organic Frameworks. *Angew. Chem., Int. Ed.* **2011**, *50*, 581−582.

(5) Furukawa, H.; Ko, N.; Go, Y. B.; Aratani, N.; Choi, S. B.; Choi, E.; Yazaydin, A. O.; Snurr, R. Q.; O'Keeffe, M.; Kim, J.; et al. Ultrahigh Porosity in Metal-Organic Frameworks. *Science (Washington, DC, U. S.)* **2010**, *329*, 424−428.

(6) Panella, B.; Hirscher, M. Hydrogen Physisorption in Metal-Organic Porous Crystals. *Adv. Mater.* **2005**, *17*, 538−541.

(7) Panella, B.; Hirscher, M.; Putter, H.; Muller, U. Hydrogen Adsorption in Metal-Organic Frameworks: Cu-MOFs and Zn-MOFs Compared. *Adv. Funct. Mater.* **2006**, *16*, 520−524.

(8) Wong-Foy, A. G.; Matzger, A. J.; Yaghi, O. M. Exceptional $H_2$ Saturation Uptake in Microporous Metal-Organic Frameworks. *J. Am. Chem. Soc.* **2006**, *128*, 3494−3495.

(9) Kaye, S. S.; Dailly, A.; Yaghi, O. M.; Long, J. R. Impact of Preparation and Handling on the Hydrogen Storage Properties of $Zn_4O$(1,4-benzenedicarboxylate)$_3$ (MOF-5). *J. Am. Chem. Soc.* **2007**, *129*, 14176−14177.

(10) Frost, H.; Düren, T.; Snurr, R. Q. Effects of Surface Area, Free Volume, and Heat of Adsorption on Hydrogen Uptake in Metal-Organic Frameworks. *J. Phys. Chem. B* **2006**, *110*, 9565−9570.

(11) Firlej, L.; Pfeifer, P.; Kuchta, B. Understanding Universal Adsorption Limits for Hydrogen Storage in Nano Porous Systems. *Adv. Mater.* **2013**, *25*, 5971−5974.

(12) Lochan, R. C.; Head-Gordon, M. Computational Studies of Molecular Hydrogen Binding Affinities: The Role of Dispersion Forces, Electrostatics, and Orbital Interactions. *Phys. Chem. Chem. Phys.* **2006**, *8*, 1357−1370.

(13) Kapelewski, M. T.; Geier, S. J.; Hudson, M. R.; Stück, D.; Mason, J. A.; Nelson, J. N.; Xiao, D. J.; Hulvey, Z.; Gilmour, E.; FitzGerald, S. A.; et al. M2 (M -Dobdc) (M = Mg, Mn, Fe, Co, Ni) Metal−Organic Frameworks Exhibiting Increased Charge Density and Enhanced H2 Binding at the Open Metal Sites. *J. Am. Chem. Soc.* **2014**, *136*, 12119−12129.

(14) Kazansky, V. B.; Pidko, E. A. A New Insight in the Unusual Adsorption Properties of Cu+ Cations in Cu-ZSM-5 Zeolite. Catal. *Catal. Today* **2005**, *110*, 281−293.

(15) Georgiev, P. A.; Albinati, A.; Eckert, J. Room Temperature Isosteric Heat of Dihydrogen Adsorption on Cu(I) Cations in Zeolite ZSM-5. *Chem. Phys. Lett.* **2007**, *449*, 182−185.

(16) Kozyra, P.; Świetek, M.; Datka, J.; Brocławik, E. Ag+ and Cu+ Cations Ligated by Zeolite Environment Enhancing Hydrogen Activation − ETS-NOCV Charge-Transfer Analysis. *J. Comput. Chem., Jpn.* **2013**, *12*, 30−37.

(17) Solans-Monfort, X.; Branchadell, V.; Sodupe, M.; Zicovich-Wilson, C. M.; Gribov, E.; Spoto, G.; Busco, C.; Ugliengo, P. Can Cu +-Exchanged Zeolites Store Molecular Hydrogen? An Ab-Initio Periodic Study Compared with Low-Temperature FTIR. *J. Phys. Chem. B* **2004**, *108*, 8278−8286.

(18) Garrone, E.; Bonelli, B.; Otero Areán, C. Enthalpy-Entropy Correlation for Hydrogen Adsorption on Zeolites. *Chem. Phys. Lett.* **2008**, *456*, 68−70.

(19) Pham, T. D.; Liu, Q.; Lobo, R. F. Carbon Dioxide and Nitrogen Adsorption on Cation-Exchanged SSZ-13 Zeolites. *Langmuir* **2013**, *29*, 832−839.

(20) Regli, L.; Bordiga, S.; Lamberti, C.; Lillerud, K. P.; Zones, S. I.; Zecchina, A. Effect of Boron Substitution in Chabazite Framework: IR Studies on the Acidity Properties and Reactivity towards Methanol. *J. Phys. Chem. C* **2007**, *111*, 2992−2999.

(21) Yun, J. H.; Lobo, R. F. Formation and Evolution of Naphthalene Radical Cations in Thermally Treated H-ZSM-5 Zeolites. *Microporous Mesoporous Mater.* **2012**, *155*, 82−89.

(22) Laugier, J.; Bochu, B. CELREF Unit-Cell refienement software http://www.ccp14.ac.uk/tutorial/lmgp/celref.htm (accessed Sep 1, 2017).

(23) Itadani, A.; Sugiyama, H.; Tanaka, M.; Mori, T.; Nagao, M.; Kuroda, Y. New Information Related to the Adsorption Model of $N_2$ on CuMFI at Room Temperature. *J. Phys. Chem. C* **2007**, *111*, 16701−16705.

(24) Lippens, B. C.; Linsen, B. G.; Boer de, J. H. Studies on Pore Systems in Catalysts I. The Adsorption of Nitrogen; Apparatus and Calculation. *J. Catal.* **1964**, *3*, 32−37.

(25) Harkins, W. D.; Jura, G. Surfaces of Solids. XIII. A Vapor Adsorption Method for the Determination of the Area of a Solid without the Assumption of a Molecular Area, and the Areas Occupied by Nitrogen and Other Molecules on the Surface of a Solid. *J. Am. Chem. Soc.* **1944**, *66*, 1366−1373.

(26) Uner, D.; Uner, M. Adsorption Calorimetry in Supported Catalyst Characterization: Adsorption Structure Sensitivity on Pt/-Al2O3. *Thermochim. Acta* **2005**, *434*, 107−112.

(27) Larson, A. C.; Von Dreele, R. B. *General Structure Analysis System (GSAS)*; Los Alamos National Laboratory, 1994; pp 86−748.

(28) Toby, B. H. EXPGUI, a Graphical User Interface for GSAS. *J. Appl. Crystallogr.* **2001**, *34*, 210−213.

(29) Hudson, M. R.; Queen, W. L.; Mason, J. A.; Fickel, D. W.; Lobo, R. F.; Brown, C. M. Unconventional, Highly Selective CO2 Adsorption in Zeolite SSZ-13. *J. Am. Chem. Soc.* **2012**, *134*, 1970−1973.

(30) Kapko, V.; Dawson, C.; Treacy, M. M. J.; Thorpe, M. F. Flexibility of Ideal Zeolite Frameworks. *Phys. Chem. Chem. Phys.* **2010**, *12*, 8531−8541.

(31) Valerio, G.; Plévert, J.; Goursot, A.; di Renzo, F. Modeling of Boron Substitution in Zeolites and Implications on Lattice Parameters. *Phys. Chem. Chem. Phys.* **2000**, *2*, 1091−1094.

(32) Drake, I. J.; Zhang, Y.; Briggs, D.; Lim, B.; Chau, T.; Bell, A. T. The Local Environment of Cu + in Cu-Y Zeolite and Its Relationship to the Synthesis of Dimethyl Carbonate. *J. Phys. Chem. B* **2006**, *110*, 11654−11664.

(33) Zhang, Y.; Drake, I. J.; Bell, A. T. Characterization of Cu-ZSM-5 Prepared by Solid-State Ion Exchange of H-ZSM-5 with CuCl. *Chem. Mater.* **2006**, *18*, 2347−2356.

(34) Guidry, T. F.; Price, G. L. The Conversion of 1-Propanamine on Copper-Containing MFI and BEA Zeolites Prepared by Aqueous and Vapor Ion-Exchange. *J. Catal.* **1999**, *181*, 16−27.

(35) Kuroda, Y.; Yagi, K.; Horiguchi, N.; Yoshikawa, Y.; Kumashiro, R.; Nagao, M. New Light on the State of Active Sites in CuZSM-5 for the NO Decomposition Reaction and N2 Adsorption. *Phys. Chem. Chem. Phys.* **2003**, *5*, 3318.

(36) Sen, D.; Kim, C. W.; Heo, N. H.; Seff, K. Using CuCl Vapor to Ion Exchange Copper into Zeolite Na-Y. Single Crystal Structure of \| Cu30Na30Cl9\|[Si 121Al71O384]-FAU Containing Cu16Cl7 21+, Cu4Cl7+, Cu3Cl2+, and Cu2+. *Microporous Mesoporous Mater.* **2014**, *185*, 16−25.

(37) Palomino, G. T.; Bordiga, S.; Zecchina, A.; Marra, G. L.; Lamberti, C. XRD, XAS, and IR Characterization of Copper-Exchanged Y Zeolite. *J. Phys. Chem. B* **2000**, *104*, 8641−8651.



DOI: 10.1021/acs.jpcc.7b09963
J. Phys. Chem. C 2018, 122, 540−548

(38) Spoto, G.; Zecchina, A.; Bordiga, S.; Ricchiardi, G.; Martra, G.; Leofanti, G.; Petrini, G. Cu(I)-ZSM-5 Zeolites Prepared by Reaction of H-ZSM-5 with Gaseous CuCl: Spectroscopic Characterization and Reactivity towards Carbon Monoxide and Nitric Oxide. *Appl. Catal., B* **1994**, *3*, 151−172.
(39) Li, Z.; Xie, K.; Slade, R. C. T. Studies of the Interaction between CuCl and HY Zeolite for Preparing Heterogeneous CuI Catalyst. *Appl. Catal., A* **2001**, *209*, 107−115.
(40) Zhang, Y.; Drake, I. J.; Briggs, D. N.; Bell, A. T. Synthesis of Dimethyl Carbonate and Dimethoxy Methane over Cu-ZSM-5. *J. Catal.* **2006**, *244*, 219−229.
(41) Sculley, J.; Yuan, D.; Zhou, H.-C. The Current Status of Hydrogen Storage in Metal−organic Frameworks—updated. *Energy Environ. Sci.* **2011**, *4*, 2721.
(42) Zacharia, R.; Cossement, D.; Lafi, L.; Chahine, R. Volumetric Hydrogen Sorption Capacity of Monoliths Prepared by Mechanical Densification of MOF-177. *J. Mater. Chem.* **2010**, *20*, 2145.
(43) Sumida, K.; Horike, S.; Kaye, S. S.; Herm, Z. R.; Queen, W. L.; Brown, C. M.; Grandjean, F.; Long, G. J.; Dailly, A.; Long, J. R. Hydrogen Storage and Carbon Dioxide Capture in an Iron-Based Sodalite-Type Metal−organic Framework (Fe-BTT) Discovered via High-Throughput Methods. *Chem. Sci.* **2010**, *1*, 184.
(44) Smith, L. J.; Eckert, H.; Cheetham, A. K. Site Preferences in the Mixed Cation Zeolite, Li,Na-Chabazite: A Combined Solid-State NMR and Neutron Diffraction Study. *J. Am. Chem. Soc.* **2000**, *122*, 1700−1708.
(45) Pham, T. D.; Hudson, M. R.; Brown, C. M.; Lobo, R. F. Molecular Basis for the High CO2 Adsorption Capacity of Chabazite Zeolites. *ChemSusChem* **2014**, *7*, 3031−3038.
(46) Shang, J.; Li, G.; Singh, R.; Gu, Q.; Nairn, K. M.; Bastow, T. J.; Medhekar, N.; Doherty, C. M.; Hill, A. J.; Liu, J. Z.; et al. Discriminative Separation of Gases by A "molecular Trapdoor" mechanism in Chabazite Zeolites. *J. Am. Chem. Soc.* **2012**, *134*, 19246−19253.



DOI: 10.1021/acs.jpcc.7b09963
*J. Phys. Chem. C* 2018, 122, 540−548